Engineering Notes

ENGINEERING NOTES are short manuscripts describing new developments or important results of a preliminary nature. These Notes cannot exceed 6 manuscript pages and 3 figures; a page of text may be substituted for a figure and vice versa. After informal review by the editors, they may be published within a few months of the date of receipt. Style requirements are the same as for regular contributions (see inside back cover).

Pressure Distribution about a Finite Axisymmetric Nacelle

DARRYL J. TRULIN* AND JAMES D. IVERSEN†
Iowa State University, Ames, Iowa

SEVERAL methods to mathematically predict the flowfields about arbitrary aerodynamic bodies now exist. One particularly successful method for axisymmetric, incompressible flowfields is contained in the Douglas' Neumann Program.[1] However, as Smith and Pierce[1] point out, a difficulty in calculation occurs when applying this program to the inlet problem. By altering the aft shape of the cowl into a semi-infinite afterbody, the forward pressure distribution on the inlet was successfully predicted.[2]

The Douglas method of solution consists of mathematically representing the axisymmetric body by a series of connected conical frustum surfaces. Each frustum surface is a source or sink sheet having a constant, but initially unknown, strength. The usual tangential flow condition is specified at each frustum midpoint. This flow requirement is expressed as a linear algebraic equation in terms of the unknown strengths with complex geometry-dependent coefficients. Since there is an equal number of midpoint equations and unknown strengths, the set of linear algebraic equations may be solved. The resulting source-sheet strengths are then used to compute the velocity and consequently the pressure distribution on the body.

In an analogous fashion, the cowl surface may be represented by frustum sheets of vorticity. In the present procedure, rather than use sheets of constant strength, a linear variation of vortex-sheet strength on each frustum with respect to its surface length is employed. The vortex-sheet strengths on coincident bases of adjacent frustums are required to be identical. Thus, a continuous variation of sheet strength exists around the cowl section with the possible exception of a discontinuity at the trailing edge. Although the linear variation of strengths makes the derivation of equations more complex, it is felt that the number of discrete input data points required may be decreased from the number used in the constant strength procedure without losing accuracy. The choice of a vortex-sheet representation instead of the source-sink sheet surface procedure allows circulation about the cowl section without necessitating the addition of a separate ring vortex.

To find the velocity components due to a single frustum of vorticity, the well-known ring vortex equations are integrated across the frustum surface. If the point in question does not lie on the frustum surface, Gaussian quadrature formulas are used to numerically integrate the ring equations. If the point lies on the frustum surface, the integrals are improper and a numerical integration is performed in a manner analogous to that used by Smith and Pierce.[1] The resulting velocity component equations derived[3] for the midpoint of the frustum shown in Fig. 1 are

$$u = \int_{-S_1}^{S_1} \frac{\gamma}{2\pi[X^2 + (1+R)^2]^{1/2}} \times \left\{K - E\left[1 + \frac{2(1-R)R}{X^2 + (1-R)^2}\right]\right\} dS =$$

$$\frac{\gamma_2}{4\pi}\left\{2\sin\beta + S_1\left[\ln\frac{8}{S_1} + \sin^2\beta\right] + \frac{S_1^2}{3}\left[\frac{13}{24}\sin\beta - \frac{1}{4}\sin\beta\ln\frac{8}{S_1} - \frac{1}{4}\sin^2\beta\right] + \frac{S_1^3}{3}\left[\frac{3}{16} - \frac{3}{16}\ln\frac{8}{S_1} + \frac{1}{4}\sin^2\beta\ln\frac{8}{S_1} - \frac{23}{48}\sin^2\beta + \frac{1}{8}\sin^4\beta\right]\right\} + \frac{\gamma_1}{4\pi}\left\{-2\sin\beta + S_1\left[\ln\frac{8}{S_1} + \sin^2\beta\right] - \frac{S_1^2}{3}\left[\frac{13}{24}\sin\beta - \frac{1}{4}\sin\beta\ln\frac{8}{S_1} - \frac{1}{4}\sin^2\beta\right] + \frac{S_1^3}{3}\left[\frac{3}{16} - \frac{3}{16}\ln\frac{8}{S_1} + \frac{1}{4}\sin^2\beta\ln\frac{8}{S_1} - \frac{23}{48}\sin^2\beta + \frac{1}{8}\sin^4\beta\right]\right\} \quad (1)$$

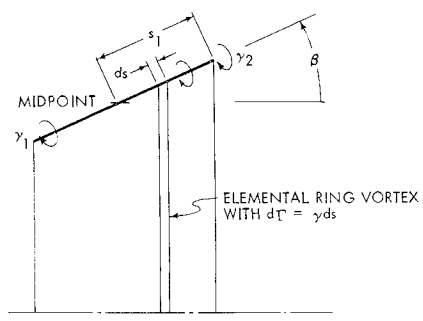

Fig. 1 Geometry of elemental frustum.

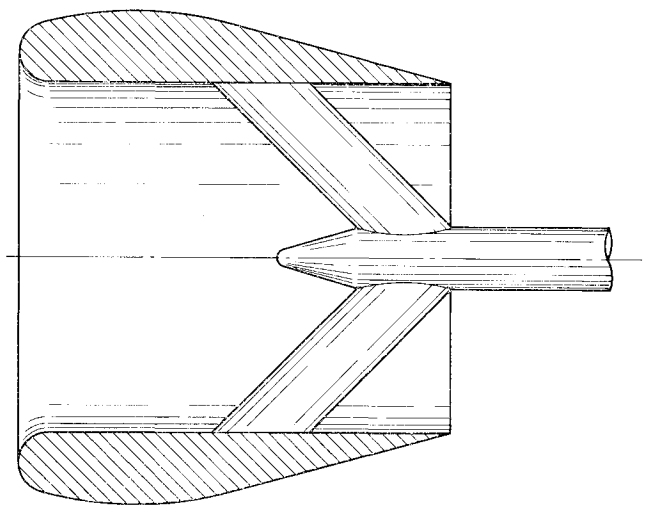

Fig. 2 Nacelle shape used to provide experimental verification of analytical results from computer program.

Received July 25, 1969.

* Assistant Professor, Department of Aerospace Engineering, Engineering Research Institute; now with General Dynamics, Pomona, Calif. Member AIAA.

† Professor, Department of Aerospace Engineering, Engineering Research Institute. Member AIAA.

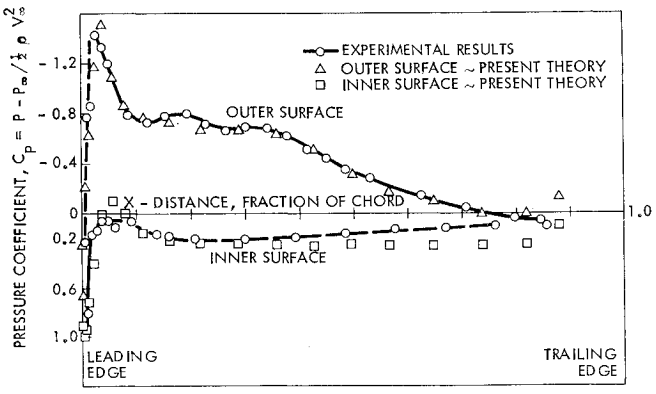

Fig. 3 Nacelle pressure distribution.

$$v = \int_{-S_1}^{S_1} \frac{(-X)\gamma}{2\pi[X^2 + (1+R)^2]^{1/2}} \times \left\{K - E\left[1 + \frac{2R}{X^2 + (1-R)^2}\right]\right\} dS =$$

$$\frac{\gamma_2}{4\pi}\left\{2\cos\beta + \sin\beta\cos\beta S_1 + \frac{S_1^2}{3}\left[\frac{3}{8}\cos\beta - \frac{\sin^2\beta}{4}\cos\beta - \frac{3}{4}\cos\beta\ln\frac{8}{S_1}\right] + \frac{S_1^3}{3}\left[\frac{\sin^3\beta\cos\beta}{8} - \frac{9}{16}\sin\beta\cos\beta + \frac{3}{8}\cos\beta\sin\beta\ln\frac{8}{S_1}\right]\right\} + \frac{\gamma_1}{4\pi}\left\{-2\cos\beta + \sin\beta\cos\beta S_1 - \frac{S_1^2}{3}\left[\frac{3}{8}\cos\beta - \frac{\sin^2\beta}{4}\cos\beta - \frac{3}{4}\cos\beta\ln\frac{8}{S_1}\right] + \frac{S_1^3}{3}\left[\frac{\sin^3\beta\cos\beta}{8} - \frac{9}{16}\sin\beta\cos\beta + \frac{3}{8}\cos\beta\sin\beta\ln\frac{8}{S_1}\right]\right\} \quad (2)$$

The velocity components u and v are in the axial and radial directions, respectively. The dimensionless coordinates X, R, and surface distance S are measured with respect to the frustum center. K and E are elliptic integrals of the first and second kinds, respectively, with moduli as functions of X and R. These equations do not account for the local surface strength at the midpoint and the term $\pm(\gamma_1 + \gamma_2)/4$ must be added to the tangential component. The sign choice depends on whether the point used is on the interior or exterior of the frustum surface.

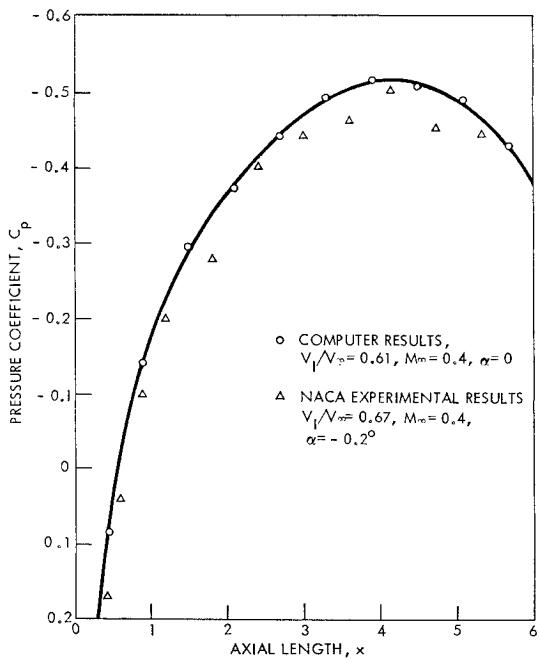

Fig. 4 Pressure distribution on the external surface of an NACA 1-60-050 nacelle section with a high mass flow.

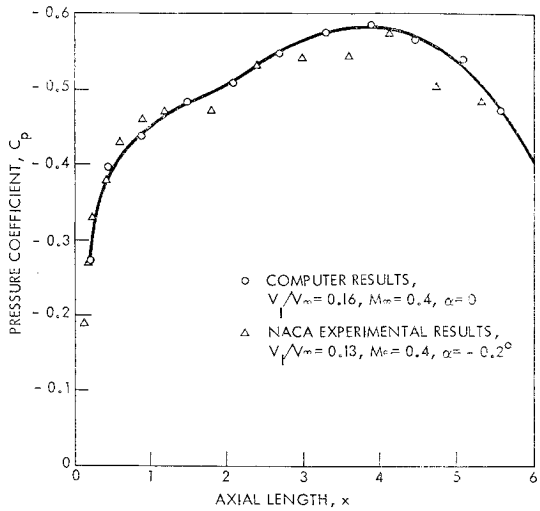

Fig. 5 Pressure distribution on the external surface of an NACA 1-60-050 nacelle section with a low mass flow.

This formulation using a linear variation of sheet strength yields a set of linear algebraic tangential flow equations similar to the Douglas method, except that there is one less frustum midpoint equation than unknown frustum base vortex sheet strengths. This deficiency of an equation allows the introduction of a modified Kutta condition at the trailing edge. A point just off the edge is chosen and an initial guess is made for the slope of the velocity vector at that point. A simultaneous solution of the resulting equations for the vortex sheet strengths is used to obtain the velocity and pressure distribution about the body. An iteration on the velocity vector slope is made if the inner and outer cowl pressures at the trailing edge are not approximately equal.

Results

The accuracy of this program was checked by building and testing the cowl shown in Fig. 2. The experimental and theoretical pressure coefficients for this cowl are plotted in Fig. 3. The greatest deviation between the two results occurs on the inner portion of the cowl. By using very approximate methods to account for the boundary-layer displacement thickness and the reduction in internal flow area due to the struts and center support, a close agreement between the experimental values and the corrected theoretical values was obtained.

A further check on the program was performed by comparing program results with experimental results[4] on an NACA 1-60-050 inlet at two different velocity ratios (V_I/V_∞, where V_I is the average axial velocity at the inlet). To simulate different velocity ratios within the program, the arbitrary choice of the velocity vector slope at the trailing edge point was varied until the desired ratio was obtained. The Gothert rule correction was used to account for the compressibility effects since the experimental values were obtained at a freestream Mach number of 0.4. High- and low-velocity ratios are shown in Figs. 4 and 5.

References

[1] Smith, A. M. O. and Pierce, J., "Exact Solution of the Neumann Problem. Calculations of Noncirculatory Plane and Axially Symmetric Flows about or within Arbitrary Boundaries," Rept. ES 26988, April 1958, Douglas Aircraft Co. Inc., Long Beach, Calif.

[2] Faulkner, S., Hess, J. L., and Giesing, J. P., "Comparison of Experimental Pressure Distributions with those Calculated by the Douglas Neumann Program," Rept. LB 31831, Dec. 1964, Douglas Aircraft Co. Inc., Long Beach, Calif.

[3] Trulin, D. J., "A Method for Computing the Pressure Distribution about an Axisymmetric Nacelle in Subsonic Flow," Ph.D. thesis, 1968, Dept. of Aerospace Engineering, Iowa State University, Ames, Iowa.

[4] Beals, D. D. and Smith, N. F., "The Development and Application of High-Critical-Speed Nose Inlets," Rept. 920, 1948, NACA.

Heat Transfer from Impinging Gas Jets on an Enclosed Concave Surface

VYTAUTAS J. JUSIONIS*
Lockheed-California Company, Burbank, Calif.

Nomenclature

A_j = cross-sectional area of a jet exhaust hole
C_p = gas specific heat
C_D = discharge coefficient
d = jet nozzle diameter
d^* = effective jet nozzle diameter
D = distance from jet nozzle to impinged surface
$f(\theta)$ = influence coefficient of angular displacement on Nu_s^*
h = heat-transfer coefficient
h_l = local heat-transfer coefficient
h_{ave} = average heat-transfer coefficient
k = gas thermal conductivity
L = the axial peripheral length of the external skin of the model
Nu_s^* = Nusselt number for internal heat transfer, $h_{ave}S^*/k$
Pr = hot air Prandtl number evaluated at jet exhaust nozzle manifold tube total conditions, $\mu C_p/k$
$\dot{q}_w$ = wall heat flux
Re_S^* = jet nozzle Reynolds number evaluated at manifold tube total conditions, $(\dot{w}/A_jC_D)S^*/\mu$
S^* = effective slot width if jet holes were replaced by a single slot
Sp = jet nozzle hole spacing on manifold tube
T = temperature
T_g = gas temperature
$T_{g,o}$ = total gas temperature in jet exhaust manifold tube
T_w = surface temperature
$\dot{w}$ = mass flowrate per jet
X = surface length from point of impingement
θ = angular displacement of jet
μ = absolute viscosity

Introduction

RESEARCH in heat transfer on surfaces caused by impinging gas jets has been usually limited to open surfaces such as flat plates or rectangular cavities. Little work has been done on problems involving enclosed surfaces. Many applications exist where jets are presently being used in enclosed surfaces. This ranges from conditions of atmospheric icing on wing leading edges and engine inlet cowl lips to stagnation-point cooling of supersonic and hypersonic vehicle leading edges and forward surfaces. It is the intention of this Note to present a more general correlation for the solution of gas jet heat transfer in internal surfaces.

Experiment

A test program was conducted upon an experimental model with a typical enclosed surface shape that would be found in aircraft application (Fig. 1). The test section of the model was 1 ft long with a 0.032-in. aluminum external skin with axial peripheral length of 9.1 in. and a nose radius of 0.62 in. The height of the model at the rear was 2.75 in. The air jet exhaust tube was 0.75 in. inside diameter with 0.0995 in. holes spaced on 0.500 in. centers. The gas exhausted out of the bottom of the model through slots near the rear bulkhead. The pressure inside the plenum of the model was approximately 1 in. of water above atmospheric during experimentation. The model skin was highly instrumented to give dense coverage of data, especially near the point of impingement. The type of test conducted was of the transient-response type where the output of the skin thermocouples was monitored vs time.

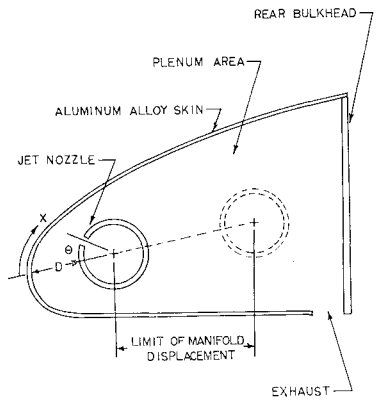

Fig. 1 Experimental model.

Three parameters were varied; the gas flow rate, the distance of the jet exhaust holes from the model skin, and the angle of inclination of the jet exhaust holes. The range of parameters tested included; air mass flow rate from 1.0 to 6.0 lb/min/ft length of jet exhaust tube manifold; distance of jet exhaust holes from model skin from 0.75 to 2.0 in.; angle of jet exhaust hole inclination from $+20°$ to $-20°$.

Results

The resulting correlation from the aforementioned test results for the average heat transfer over the skin surface is

$$Nu_s^* = 0.030\, f(\theta)(D/S^*)^{-0.4} Re_s^{*0.7}\, Pr^{0.3} \quad (1)$$

The heat-transfer coefficient is defined in terms of the gas total temperature found inside the jet nozzle manifold tube rather than an arrival temperature found near the impinged surface. The total temperature is a more well defined or known quantity while performing analysis and eliminates the error incurred when calculating an arrival temperature. The heat-transfer coefficient is therefore defined as

$$h = \dot{q}_w/(T_{g,o} - T_w) \quad (2)$$

The angular dependence function is given as

$$f(\theta) = 0.087\,(2^{1+\theta/20}) + 0.826 \quad (3)$$

Equation (1) has been cast into such a form that the hole spacing (or slot) and hole diameter on the jet exhaust manifold tube is replaced by an effective two-dimensional slot of width S^*. This eliminates the need for another parameter to take into account hole spacing and hole diameter:

$$S^* = \pi(d^*)^2/4Sp \quad (4)$$

The contraction coefficient is incorporated into the effective hole diameter d^*:

$$d^* = d(C_D)^{1/2} \quad (5)$$

Equation (1) is valid over the range of independent parameters and geometrical variables as shown in Table 1. For symmetrical external surfaces, the author suggests that θ in the angular correction term be replaced by $|\theta|$ in Eq. (3). A comparison with test data is plotted in Fig. 2.

Received July 7, 1969.

* Thermodynamics Engineer; now at U. S. Air Force Headquarters SAMSO, Los Angeles, Calif. Member AIAA.